Journal of Physics: Conference Series

PAPER • OPEN ACCESS

Optical wavefields measurement by digital holography methods

To cite this article: M S Kovalev *et al* 2018 *J. Phys.: Conf. Ser.* **1096** 012112

View the article online for updates and enhancements.

You may also like

- Thermooptics of magnetoactive media: Faraday isolators for high average power lasers
E A Khazanov
- Adaptive optics in the formation of optical beams and images
V P Lukin
- Peculiarities of adaptive phase correction of optical wave distortions under conditions of 'strong' intensity fluctuations
V.P. Lukin, N.N. Botygina, O.N. Emaleev et al.

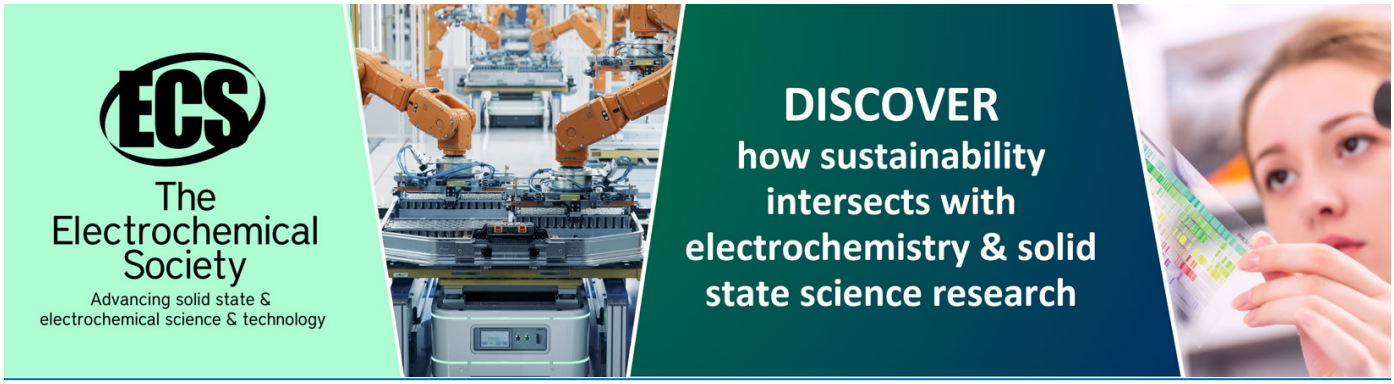

This content was downloaded from IP address 18.118.137.243 on 25/04/2024 at 23:17

Optical wavefields measurement by digital holography methods

M S Kovalev[1], G K Krasin[1], S B Odinokov[1] and A Y Zherdev[1]

[1]Bauman Moscow State Technical University, Baumanskaya Street 2, Moscow, Russia, 105005

e-mail: m.s.kovalev@gmail.com, krasin.georg@gmail.com

Abstract. The phase distortions arise due to the atmospheric turbulence, the experimental conditions or a low quality of the imaging system. They can seriously limit the resolution of the image. Phase distortions can be spatially dependent, which means that a linear space-invariant transfer function cannot completely correct all phase errors in the field of view. Computer holography can be used to access a complex-valued optical field from an object under coherent illumination after detecting interference of intensity between the object and the reference beams. In this work, we developed approaches to improve image sharpness to measure phase distortions in computer holography using the example of defocus measurement. Image enhancement algorithms use a nonlinear optimization procedure to determine and measure phase distortions to form a reconstructed image at a high resolution. Our work was focused on numerical modelling, developing algorithms and conducting laboratory experiment.

1. Introduction

The investigations of laser wavefields are popular nowadays because they can help to solve many research and application tasks in the field of modern photonics systems.

Firstly, these are the tasks of optical meteorology, in which some physical characteristics of an object should be determined. These are the such characteristics [1-6] as the surface shape, the refraction index, optical thickness etc. The characteristics are required for the creation of precise optical systems and devices [7-9] and can be determined with the help of measured parameters of an optical wave from the radiation source that has passed through the object or has reflected from its surface. Secondly, there are tasks that contain the determination of characteristics of the optical radiation formed with some external sources. These tasks are prior in laser physics where the quality control tests are necessary after the generation of laser beams [8] and during the construction of different adaptive systems. Furthermore, while solving certain technical tasks, the wavefield with required spatial characteristics [2, 10-12] should be formed.

The main problem in the research of the laser wavefields is the registration of their spatial amplitude-phase distribution because the devices that measure straight phase distortions haven't been invented yet. For sure, nowadays there are some methods that make it possible to register the profile of a phase front and to look into wavefield that have been formed by different light sources. The most developed devices are interferometers [6] and sensors based on the Hartmann [13, 14] and Shack–Hartmann methods. The most precious results in the study of laser wavefields were obtained with the help of different interferometers. However, they can determine only the phase difference of two coherent light beams. One of them is a reference beam, what essentially bound the field of their application. Other phasometric methods are much inferior in accuracy to the interferometric ones and

Content from this work may be used under the terms of the Creative Commons Attribution 3.0 licence. Any further distribution of this work must maintain attribution to the author(s) and the title of the work, journal citation and DOI.
Published under licence by IOP Publishing Ltd

also do not give a satisfactory solution to the task of recording the optical wavefield. As the result, the task of invention of alternative methods for measurements of phase distortions of light field is still popular.

It is proposed to use computer holography principles for the measurements of the phase distortions [15-24]. In this case the main issue in this case will be intermodal cross-talk noise [25]. The computer synthesis of holograms is based on a mathematical representation of fundamental principles of optical holography [26]. The synthesis started developing at the same time as computing technics and such software tools as fast Fourier transformation were improving.

Nowadays a personal computer and a computing tool installed on it make it possible to calculate computer-generated holograms (CGHs) for a specific task. It is widely thought that the advantage of the computer synthesis method is that it eliminates the necessity to photochemically record the holograms. Moreover, the method makes it possible to reconstruct it numerically in real time; to better the quality of a reconstructed image with the help of many methods of digital image processing; and to use these dynamically changing CGHs in optical sensors and correction systems of optical remedies. The ability to use phase distribution function that is expressed by Zernike polynomial representation [27, 28] as a virtual object makes it possible to determine interferential interaction of aberration wavefronts and plane waves of any difficulty. When working with CGHs that are recorded on a photosensitive material, certain restrictions appear because of a small dynamic range. To increase the range of distinguishable aberrations, the introduction of such a dynamically changing transparency, for example, an LCD spatial light modulator, is required. In this case the wavefront sensor will inevitably be connected to a massive electronic control unit; but the achieved preciousness worths it. The determination of aberrations is intended to be carried out according to a widely known principle of "coarse-accurate" scale, in which a preliminary rapid analysis determines an aberration type and then their size is analyzed with an accurate adjustment.

2. Principles of calculating the CGH

CGH is an intensity distribution from two waves – a reference r(x,y) and an object o(x,y) waves. The synthesis and reconstruction of the CGH is shown on the figure 1. In this case, the reference wave is an aberrated wavefront, the object wave is a field from an indicator point. In this way if a value of an aberration in an incident wave and the CGH are matched we'll get a small indicator point. Otherwise the point will be blurred.

The intensity of the transparence function is determined by a combination of the reference and the object waves:

$$I(\mu,\nu) = |O(\mu,\nu) + R(\mu,\nu)|^2 = |R(\mu,\nu)|^2 + |O(\mu,\nu)|^2 + O(\mu,\nu)R^*(\mu,\nu) + O^*(\mu,\nu)R(\mu,\nu) \quad (1),$$

where $O(\mu,\nu)$ – field of the object wave, $R(\mu,\nu)$ – field of the reference wave, the sign * means complex conjugate.

$$O(\mu,\nu) = \mathcal{F}\{o(x,y)\} = \mathcal{F}\{|o(x,y+\Delta)|\exp(i\varphi_0(x,y))\} \quad (2)$$

Equation (2) shows the field of the object wave which is calculated by Fourier transform of the complex amplitude of the object wave. Here $|o(x,y+\Delta)|$ is a real amplitude and $\varphi_0(x,y)$ is a phase of the wave.

$$R(\mu,\nu) = \mathcal{F}\{r(x,y)\} = \mathcal{F}\{|r(x,y)|\exp(i\varphi_0(x,y))\} \quad (3)$$

Equation (3) similarly shows the field of the reference wave.

The initial object wave can be reconstructed when the CGH is illuminated by the reference wave. To reconstruct the image we should multiply the recorded CGH that is interference intensity $I(\mu,\nu)$ and the field of the reference wave $R(\mu,\nu)$:

$$I(\mu,\nu)R(\mu,\nu) = |R(\mu,\nu)|^2R(\mu,\nu) + |O(\mu,\nu)|^2R(\mu,\nu) + O(\mu,\nu)|R(\mu,\nu)|^2 + R^2(\mu,\nu)O^*(\mu,\nu) \quad (4)$$

The first term in the right part of the equation (4) is proportional to a value $R(\mu,\nu)$ of the reference wave. The spatially-changing "cloud" around the first order of diffraction describes by second term. They form a zero order of diffraction or a background component together. The third term, up to a known multiplier, is an exact copy of the original field $O(\mu,\nu)$ and is called virtual image of the object. The fourth term is another object image which is real image.

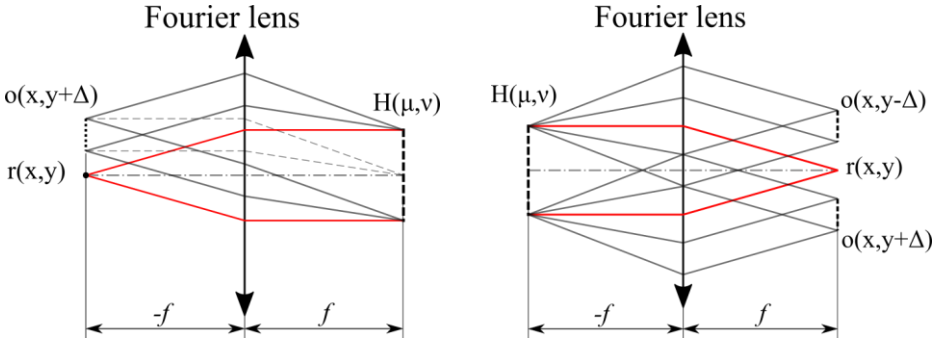

Figure 1. Principles of synthesis and reconstruction of a CGH.

3. Computer modeling

The matlab program for modeling was written. In this program from the formulas indicated above the amplitude CGHs was calculated. An object wave is the indicator point in the array of zeros. The reference wave is a plane wave with the Zernike polynomial as a phase multiplier inside. On the figure 2 one can see amplitude CGH for defocus aberration. The CGHs are a diffraction grating on which the Zernike polynomial is applied. The carrier frequency of the diffraction grating is determined by a position of the indicator point. The closer the indicator point to the center, the lower the carrier frequency of the diffraction grating. But due to the negative effect of zero order one cannot place the indicator point too close to the center.

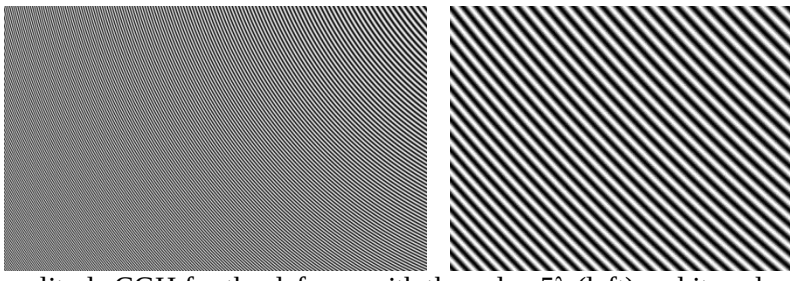

Figure 2. The amplitude CGH for the defocus with the value 5λ (left) and its enlarged part (right).

Further in the program the reconstruction of such CGH is calculated. At first the reconstruction of the CGH was tested by a reference wave with the same aberration value as in the CGH. On the figure 3 one can see the result of the reconstruction of the amplitude CGH. In the +1 order of the reconstructed image, one can see the point of diffraction size (figure 3a). This means that the aberration values in the CGH and in an incident wave coincide. Then the CGH was changed to determine the minimum detectable value of the phase distortion. In this case the indicator point was blurred (figure 3b). The minimum detectable value of the phase distortion was λ/35. This value is constant for the entire dynamic range, which was verified by modeling from 0.01λ to 10λ.

By reconstructing an amplitude CGHs, three diffraction orders can be obtained. Zero order, which doesn't contain any useful information and ± 1 diffraction orders (figure 3). By reconstructing a phase CGHs more diffraction orders can be obtained. In case of phase CGHs the new phenomenon was discovered, which can be applied to an aberration measurement. The indicator point moves to +2 order (figure 4a), when a phase CGH is illuminated by reference wave with the aberration value two times larger than in the CGH. The indicator point moves to the +3 order (figure 4b), when the aberration value in the reference wave is three times larger. Further, the diffraction efficiency falls and it becomes impossible to recognize the image of the indicator point. One can accelerate the algorithm for measuring aberrations with the help of this phenomenon.

From the figure 2, one can see that the CGHs are grayscale. We have also concluded modeling with a binary CGHs. The result is shown on the figure 5. In this case, the minimum detectable value of the phase distortion remains unchanged, although the diffraction efficiency has increased. Also the zero order of diffraction as well as all even orders have disappeared. This means that all energy is distributed in uneven diffraction orders.

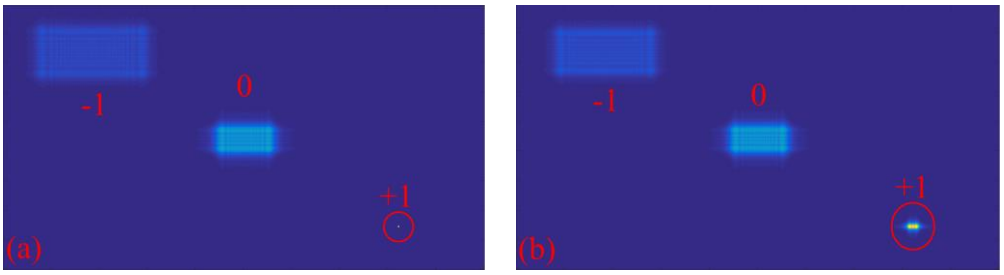

Figure 3. Reconstructed images for 6λ defocused wave and grayscale defocusing aberration CGHs of 6λ (a) and 5λ (b) value.

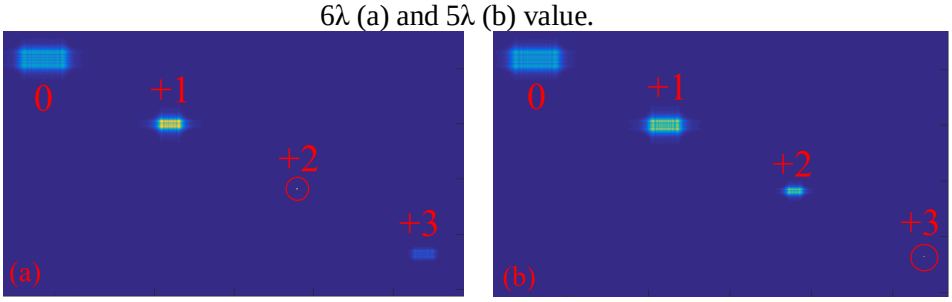

Figure 4. Reconstructed images for 6λ defocused wave and phase grayscale defocusing aberration CGHs of 3λ (a) and 2λ (b) value.

It was not possible to repeat the experiment with moving of the indicator point in the diffraction orders with binary CGHs. However, the binary CGHs can simplify the physical experiments. It is necessary to know the phase characteristic of the spatial light modulator when using grayscale GCHs. While there isn't such a problem for binary CGHs. Thus, binary CGHs, in addition to enhanced diffraction efficiency, are preferred for use in further physical experiments.

The CGHs was calculated for four different types of aberrations: defocus, coma, astigmatism and spherical aberration. And the phenomenon indicated above was obtained for all of them. But further experiments was implemented for defocus aberration due to simplicity of introducing it in the optical scheme.

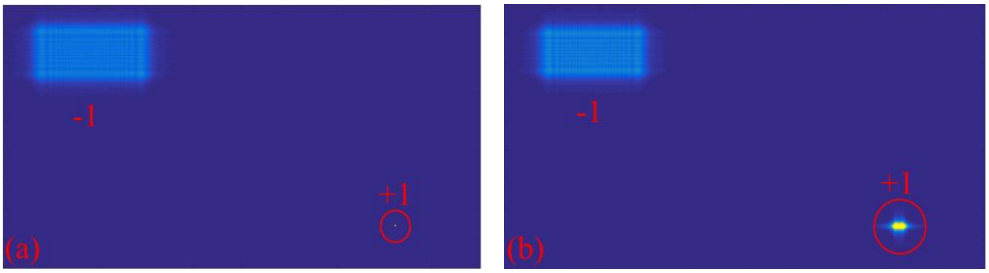

Figure 5. Reconstructed images for 6λ defocused wave and binary defocusing aberration CGHs of 6λ (a) and 5λ (b) value.

4. Experimental studies

For examination of a proposed method an experimental optical setup was designed. The optical scheme of this stand is shown in figure **6**. The experimental setup consists of a laser, a telescopic expanding system with a pinhole, a display, a Fourier lens and a screen.

Laser light reflected by two mirrors is falling to the telescopic system. The telescope expands light wave diameter to the size of the SLM. A pinhole is used to clean wave and form plane wave front with aberrations less than 0.01λ. Next wave falls at the SLM, where CGHs are displayed. In the end the screen is placed in the focal plane of the Fourier lens. A reconstructed image is located at the screen.

The experimental setup is shown in figure **7**. We use a He–Ne laser with wavelength of 633 nm. The telescopic system consists of a microscope 20$^{\times}$ lens, a 20 μm pinhole and a lens with focal length of 250 mm. The SLM PLUTO VIS (420–650 nm) was used to display CGHs. The Fourier lens has focal length 1 000 mm.

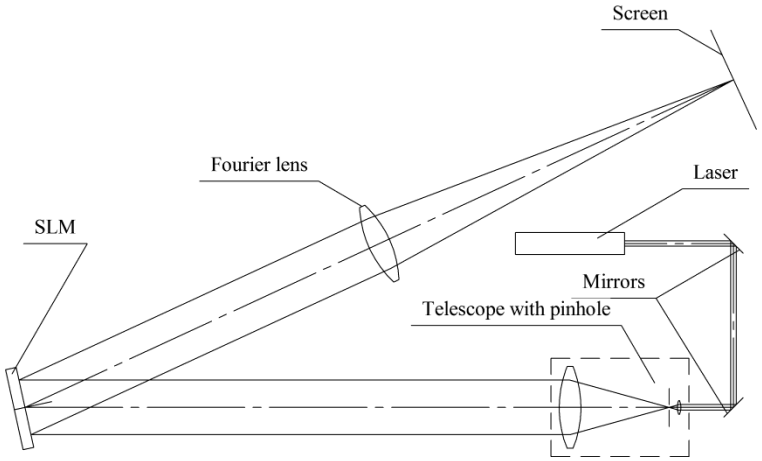

Figure 6. The optical scheme of the experimental setup.

During experimental studies calculated CGHs was displayed at the SLM and reconstructed images was captured by a camera. We examine three grayscale CGHs (figure **9**) and three binary CGHs (figure **10**). Before experiments an image of plane wave focusing dot and aberrated wave focusing dot was captured (figure **8**). While we was investigating focusing dot a solid white field was displayed at the SLM.

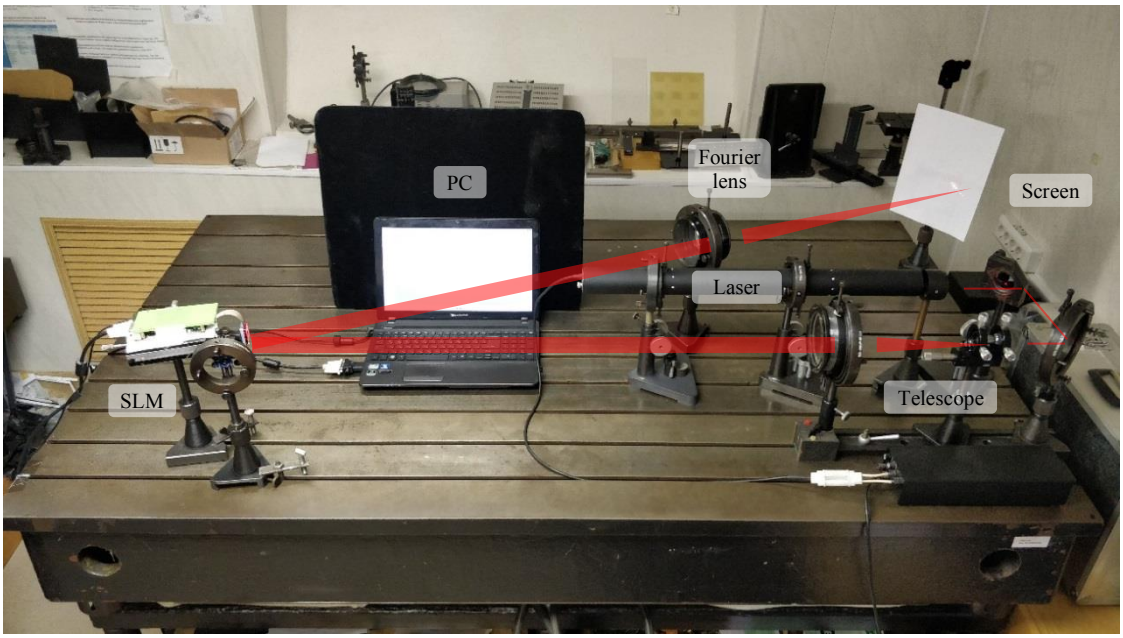

Figure 7. The photo of the experimental setup.

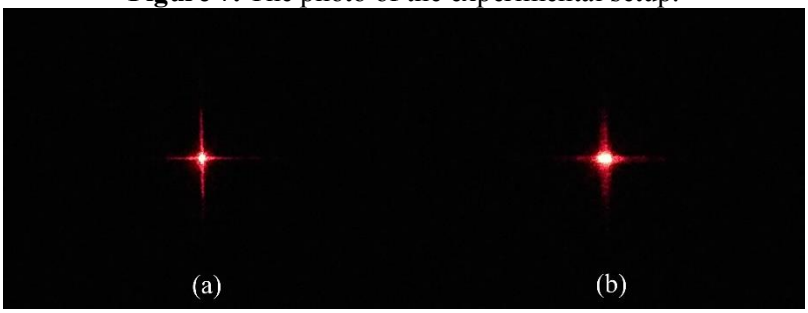

Figure 8. A focusing dot for a plane wave (a) and for a wave with 5λ defocusing aberration (b) without a CGH at the SLM.

In figure 8 one can see, that plane wave without aberrations has a narrow focusing dot with cross caused by diffraction at the SLM aperture (figure 8a). Diffraction orders caused by diffraction at the SLM structure is out of the image field. Next we add defocusing aberration in the wave by moving the microscope lens with the pinhole from the second lens along optical axis. Adding of defocusing leads to blurring of focusing dot and cross (figure 8b).

The value of the reference wave defocusing is 6λ. Further experiments was carried out with this defocusing reference wave and CGHs displayed at SLM.

Images reconstructed from grayscale CGHs for defocusing of 6λ, 3λ, 2λ by defocusing wave are shown in figure 9. The reconstructed image for the 6λ defocusing CGH has the indicator point in the +1 order as it was expected (figure 9a). The indicator point has a shape of narrow dot with smallest diameter. All other orders have a rectangular shape of greater size.

Reconstructed images for 3λ and 2λ defocusing grayscale CGHs have indicator points in +2 and +3 order dots accordingly (figure 9b and 9c).

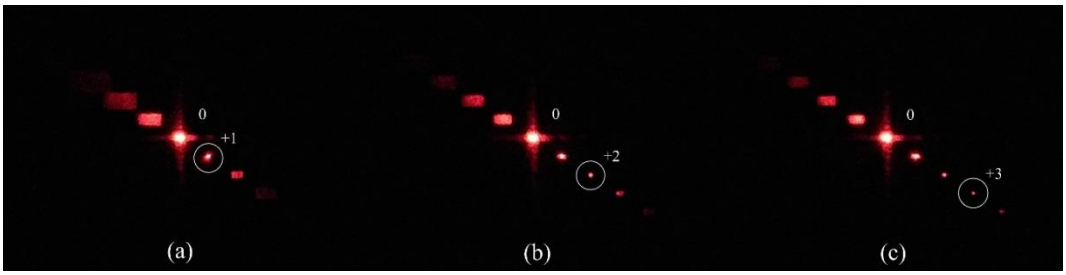

Figure 9. Reconstructed images for 6λ defocused wave and grayscale defocusing aberration CGHs of 6λ (a), 3λ (b) and 2λ (c) value.

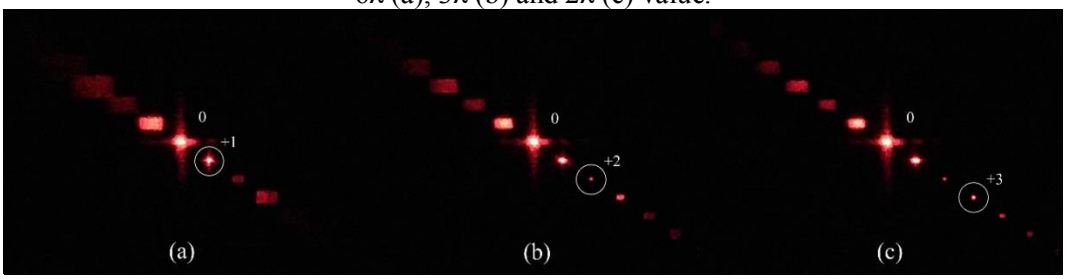

Figure 10. Reconstructed images for 6λ defocused wave and binary defocusing aberration CGHs of 6λ (a), 3λ (b) and 2λ (c) value.

Images reconstructed from binary CGHs for defocusing of 6λ, 3λ, 2λ by defocusing wave are shown in figure 10. The reconstructed image for the 6λ defocusing CGH has the indicator point in the +1 order (figure 10a). For binary CGHs reconstructed images have greater amount of visible orders due to lower energy level of the zero order dot.

The reconstructed image for the 3λ defocusing binary CGHs has the indicator point in the +2 order (figure 10b), but this dot has low level as it is an even order. The reconstructed image for the 2λ defocusing binary CGHs must has the indicator point in the +3 order (figure 10c), but the +2 order dot still has a smaller diameter after a smaller energy level.

The measurement of aberrations is intended to be carried out according to a principle of "coarse-accurate" scale as was said above. CGHs with a big increment of aberration value recorded on them are outputted successively on the LCD SLM. After the approximate aberration definition of the aberration value CGHs with a smaller step is outputted. So, in the first case it is 1λ, then 2λ etc. After that the step will decrease to 0.1λ, for example 3.1λ, then 3.2λ. And lastly, step will decrease to 0.01λ to increase accuracy. Each of the aberration will be measured one at a time. After determining one of aberration algorithm will move to the next. Although time of measurement will increase, we can exclude intermodal cross-talk noise. Intermodal cross-talk noise is an issue of all holographic wavefront sensors, which can decrease the precision and induce errors. Also using the newfound phenomenon can decrease the time of measurement.

5. Conclusion

A new method for plane wave aberration measuring is proposed. The method is based on theoretically described and calculated phenomenon of indicator point shifting to higher diffraction orders while wave aberration is controlled with CGH setting up on divider value. This phenomenon is calculated for grayscale and binary CGHs. Binary CGH show higher diffraction efficiency but even diffraction order dots in a reconstructed image have lower energy level compared with odd order dots. That makes automatic measurement more difficult compared to grayscale CGHs. Grayscale CGHs show calculated behavior and wave aberration measurement could be processed in higher diffraction orders of a reconsructed image for increasing of aberration value resolution. It can also decrease the time of measurement.

6. References

[1] Poleshchuk A G, Nasyrov R K and Asfour J-M 2016 Interferometric testing of steep cylindrical surfaces with on-axis CGHs *Computer Optics* **40(5)** 625-**62**8 DOI: 10.18287/2412-6179-2016-40-5-625-628

[2] Rozhkov O V, Piskunov D E, Nosov P A, Pavlov V Yu, Khorokhorov A M and Shirankov A F 2018 Bauman MSTU scientific school “zoom lens design”: Features of theory and practice *Computer Optics* **42(1)** 72–83 DOI: 10.18287/2412-6179-2018-42-1-72-83

[3] Machikhin A, Batshev V and Pozhar V 2017 Aberration analysis of AOTF-based spectral imaging systems *J. Opt. Soc. Am.* A **34** 1109-1113

[4] Denisov D G 2017 Error analysis in digital processing of the results of interferometric control of nano-scale local deviations of optical surfaces *Computer Optics* **41(6)** 820-830 DOI: 10.18287/2412-6179-2017-41-6-820-830

[5] Gladysheva Ya V, Zhivotovskii I V, Denisov D G and Baryshnikov N V 2016 Algorithm for reconstructing a profile of a flat high-precision optical surface *Measuring Technique* **2** 28-32

[6] Poleshchuk A, Khomutov V, Matochkin A, Nasyrov R and Cherkashin V 2016 Laser interferometers for control of optical surface shape *Photonics* **4** 38-51

[7] Fernandez T T 2017 Thermo-optical and lasing characteristics of Cr2+-doped CdSe single crystal as tunable coherent source in the mid-infrared *Opt. Mater. Express* **7** 3815-3825

[8] Katyba G M, Zaytsev K I, Rossolenko S N, Shikunova I A, Shikunov S L, Stryukov D O, Yurchenko S O and Kurlov V N 2017 Technological aspects of manufacturing terahertz photonic crystal waveguides based on sapphire shaped crystals *SPIE Conf. Proc.* **10333** 103331C

[9] Shikunova I A, Zaytsev K I, Stryukov D O, Dubyanskaya E N and Kurlov V N 2017 Neurosurgical sapphire handheld probe for intraoperative optical diagnostics, laser coagulation and aspiration of malignant brain *Proc. SPIE Clinical and Preclinical Optical Diagnostics* **10411** 104110Q

[10] Nosov P A, Pavlov V Yu, Pakhomov I I and Shirankov A F 2011 Aberrational synthesis of optical systems intended for the conversion of laser beams *Journal of Optical Technology* **78(9)** 34-44

[11] Pakhomov I I, Shirankov A F and Nosov P A 2010 Description, calculation, and analysis of the distortions of multimode laser beams *Journal of Optical Technology* **77(2)** 3743

[12] Anikanov A G, Pakhomov I I and Shirankov A F 2010 Structural synthesis of laser optical systems when their parameters are restricted *Journal of Optical Technology* **77(2)** 3036

[13] Poleshchuk A G, Sedukhin A G, Trunov V I and Maksimov V G 2014 Hartmann wavefront sensor based on multielement amplitude masks with apodized apertures *Computer Optics* **38(4)** 695-703

[14] Druzhin V V and Puryaev D T 2007 Hartmann method for monitoring the shape of convex aspheric mirrors of large optical telescopes *J. Opt. Technol.* **74** 794-796

[15] Palomo P M, Zepp A and Gładysz S Characterization of the digital holographic wavefront sensor *SPIE Conf. Proc* **9242** 92421T DOI: 10.1117/12.2067084

[16] Zepp A, Gładysz S and Stein K 2013 Holographic wavefront sensor for fast defocus measurement *Advanced Optical Technologies* **2(5-6)** 433-437 DOI: 10.1515/aot-2013-0050

[17] Anzuola E, Zepp A, Gładysz S and Stein K 2016 Holographic wavefront sensor based on Karhunen-Loève decomposition *SPIE Conf. Proc* **9979** 99790X DOI: 10.1117/12.2236341
[18] Kovalev M S, Krasin G K, Malinina P I, Odinokov S B and Sagatelyan H R 2016 Wave front sensor based on holographic optical elements *J. Phys.: Conf. Ser.* **737** 012064
[19] Bobrinev V I, Galkin M L, Kovalev M S 2018 Investigation of Computer-Generated Fresnel Holograms for Wavefront Sensors *Optoelectronics, Instrumentation and Data Processing* **54(1)** 26-31 DOI: 10.3103/S8756699018010053
[20] Kovalev M S, Krasin G K, Nosov P A, Odinokov S B and Filippov I Yu 2017 The Calculation of the Diffraction Integral Using Chebyshev Polynomials *Int. Journal of Applied Engineering Research* **12(23)** 13303-13309
[21] Gorelaya A, Kovalev M, Malinina P, Odinokov S, Soloviev M, Sevryugin A and Venediktov V 2017 Advanced holographic wavefront sensors *SPIE Conf. Proc.* **10233** 102330Z
[22] Kodatskiy B, Kovalev M S, Malinina P I, Odinokov S B, Soloviev M and Venediktov V Y 2016 Recent progress in holographic wavefront sensing *SPIE Conf. Proc.* **10022** 1002219
[23] Kodatskiy B, Kovalev M S, Malinina P I, Odinokov S B, Soloviev M and Venediktov V Y 2016 Fourier Holography in Holographic Wavefront Sensors *SPIE Conf. Proc.* **10002** 100020K
[24] Orlov V V 2017 Holographic mode wavefront sensor with an enlarged number of measured modes *Quantum Electronics* **47(8)** 773-776
[25] Gavril'eva K, Gorelaya A, Fedorov E, Pattia Matital R, Orlov V, Shubenkova E and Venediktov V 2018 Approaches to cross-talk noise reduction in modal holographic wavefront sensors *SPIE Conf. Proc.* **10680** 106802O DOI: 10.1117/12.2306472
[26] Goodman J W 2005 *Introduction to Fourier optics* (Englewood Colorado: Roberts and Co)
[27] Hopkins H H 1949 *Wave theory of aberrations* (New York: Oxford Univ. Press)
[28] Born M and Wolf E 2003 *Principles of optics* (Cambridge: Cambridge Univ. Press) 203-218

Acknowledgments
This work was performed in Bauman MSTU with financial support from the Ministry of Education and Science of the Russian Federation within the contract No. 14.577.21.0258 (Grant No. RFMEFI57717X0258).